

# Fabry-Perot fiber tip sensor based on an inner air-cavity for refractive index sensing

Guilin Zhang (张桂林)\*, Minghong Yang (杨明红), and Yutang Dai (戴玉堂)

National Engineering Laboratory for Fiber Optic Sensing Technology, Wuhan University of Technology, Wuhan 430070, China

\*Corresponding author: yingichangkong@163.com

Received August 5, 2013; accepted October 17, 2013; posted online March 25, 2014

We propose a simple and low-cost Fabry-Perot (F-P) fiber sensor based on an inner air cavity. The air cavity is fabricated at the fiber-tip by splicing a single-mode fiber and a hollow-core photonic crystal fiber (HC-PCF), with un-collapsed section of the HC-PCF being cleaved. Application of F-P fiber-tip sensor in the external refractive index (RI) measurement is experimentally demonstrated. The sensor exhibits a good linear response and high sensitivity of  $-54.409$  dB/RIU in the RI range of 1.333–1.413. Therefore, it is applied to fiber-optic biological and chemical sensing.

OCIS codes: 120.2230, 060.2370.

doi: 10.3788/COL201412.S11202.

Fiber-optic Fabry-Perot (F-P) interferometers have been widely used in the measurement of physical quantities in many fields of science and technology. Physical parameters include temperature, humidity, strain, liquid level and refractive index (RI), etc.<sup>[1–6]</sup>. The RI parameter is highly important for chemical and biological sensing. Therefore, various F-P RI sensors have been developed in the past few years. For instance, Tian *et al.* fabricated a microfluidic F-P RI sensor based on a fiber hollow tube sandwiched between two cleaved microstructured fibers<sup>[1]</sup>. Rao *et al.* also reported a novel F-P RI sensor formed by splicing a section of photonic crystal fiber (PCF) to a single-mode fiber (SMF)<sup>[2]</sup>. In addition, by utilizing the femtosecond laser, the open F-P cavity formed on SMF was directly carved. Wei *et al.* reported a miniaturized fiber in-line F-P RI sensor fabricated by one-step femtosecond laser micromachining<sup>[3]</sup>. In general, these devices have shown high RI sensitivity. However, the above fabrication processes are not simple. For these F-P RI sensors<sup>[1,3]</sup>, characterized by the wavelength shift in response to RI changes, the reliability can be affected seriously by contaminants deposited on the F-P cavity during the liquid-filling process<sup>[7]</sup>. Recently, some papers reported the novel F-P RI sensor based on a hollow glass microsphere at the fiber-tip<sup>[8,9]</sup>. The measurement technique is based on the Fresnel reflection at the fiber's cleaved end. Although the liquid-filling process is avoided, the loss of these sensors is high because of the long air cavity.

In this paper, we present a simple F-P fiber sensor used for measuring the RI of liquid at a fiber-tip. This device consists of an inner air cavity fabricated by fusion-splicing SMF and hollow-core PCF (HC-PCF) with the un-collapsed section of the HC-PCF being cleaved. The light reflected from the fiber-tip thus interferes with the light reflected from the air cavity. By measuring the fringe contrast of the interference pattern from the reflection spectrum, we can determine the

RI of the liquid accurately. As the fabrication involves only splicing and cleaving, the sensor can be easily constructed with low cost.

Figure 1 shows the fabrication process of the F-P fiber-tip sensor based on inner air cavity. Primarily, a FIBEL S177 splicer, with a semi-automatic splice mode, was used to fabricate the air cavity. To collapse the core of the HC-PCF effectively, the discharging power was set at 130 bit (the power unit is default). The gap between HC-PCF and SMF can determine the size of air cavity. After arc procedure, the air holes of HC-PCF collapsed completely over a length of a few hundred micrometers, and the air cavity was formed internally, as shown in Figs. 1(b) and (e). Then, the uncollapsed section of the HC-PCF was cleaved, and the length of collapsed

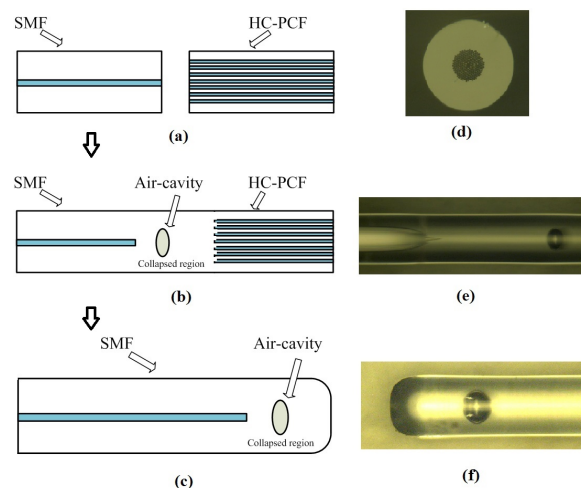


Fig. 1. Fabrication of the F-P fiber-tip sensor. (a) Fusion splicing of an SMF and a HC-PCF. (b) Cleaving the uncollapsed section of the HC-PCF. (c) Adding one arc at fiber-tip. (d) A microscope image of HC-PCF cross-section. (e) A microscope image of the joint between SMF and HC-PCF. (f) A microscope image of the F-P fiber-tip.

region can be adjusted by using cutter. At the end, to improve the fringe contrast of the interference pattern, adding one arc at fiber-tip and the end-face results in curved surface. Fig. 2(f) shows the microscope image of the F-P fiber-tip. In the whole process, only a fusion splicer and cutter were used and no additional alignment procedure was required.

Figure 2 shows the schematic diagram of the F-P RI sensor. There are three reflection surfaces in the fiber sensor head, and the corresponding power reflection coefficients are  $R_1$ ,  $R_2$  and  $R_3$ , respectively. Transmission loss factors at air cavity and collapsed region are  $\alpha_1$  and  $\alpha_2$ . Lengths of these two physical cavities are  $L_1$  and  $L_2$ . The RIs of air, fiber and liquid are  $n_0$ ,  $n_1$  and  $n_2$ , respectively. According to Fresnel formula,  $R_1$  and  $R_2$  both are equal to  $(n_1 - n_0)^2 / (n_1 + n_0)^2 = 0.034 \ll 1$ ,  $R_3$  is equal to  $(n_2 - n_1)^2 / (n_2 + n_1)^2 \ll 1$ , which depends on the RI of liquid. Considering the low reflection coefficients, higher-order reflections from these surfaces may be ignored. As a result, the normalized total reflected intensity ( $I$ ) is given by<sup>[10]</sup>

$$\begin{aligned} I &= (E_1 + E_2 + E_3)(E_1 + E_2 + E_3)^* \\ &= R_1 + (1 - \alpha_1)^2(1 - R_1)^2 R_2 + (1 - \alpha_1)^2(1 - \alpha_2)^2 \\ &\quad (1 - R_1)^2(1 - R_2)^2 R_3 + 2\sqrt{R_1 R_3}(1 - \alpha_1)(1 - \alpha_2) \\ &\quad (1 - R_1)(1 - R_2) \cos[2(\Phi_1 + \Phi_2)] + 2\sqrt{R_2 R_3} \\ &\quad (1 - \alpha_1)^2(1 - \alpha_2)(1 - R_1)^2(1 - R_2) \cos(2\Phi_2) \\ &\quad + 2\sqrt{R_1 R_2}(1 - \alpha_1)(1 - R_1) \cos(2\Phi_1), \end{aligned} \quad (1)$$

where,  $E_1$ ,  $E_2$  and  $E_3$  are the reflected electric fields of the three reflection surfaces.  $\Phi_1$  and  $\Phi_2$  ( $\Phi_1 = 4\pi n_0 L_1 / \lambda$ ,  $\Phi_2 = 4\pi n_1 L_2 / \lambda$ ) are the propagation phase shifts. According to Eq. (1), the fringe contrast of the interference pattern can be obtained as follows<sup>[2]</sup>

$$\begin{aligned} V &= \frac{I_{\max} - I_{\min}}{I_{\max} + I_{\min}} = \\ &= \frac{2\sqrt{R_1}(1 - R_1)(1 - \alpha_1)(1 - \alpha_2)(n_2 - n_1) / (n_2 + n_1)}{R_1 + (1 - \alpha_1)^2(1 - \alpha_2)^2(1 - R_1)^2[(n_2 - n_1) / (n_2 + n_1)]^2}. \end{aligned} \quad (2)$$

As the parameters  $R_1$ ,  $\alpha_1$ ,  $\alpha_2$  and  $n_1$  can be regarded as constants<sup>[10]</sup>, it is worth noting that  $V$  is only related to  $n_2$  in Eq. (2). Therefore, the RI of liquid can be obtained by measuring the fringe contrast.

Figure 3(a) shows the schematic diagram of the experimental setup for measuring RI. A light-emitting diode

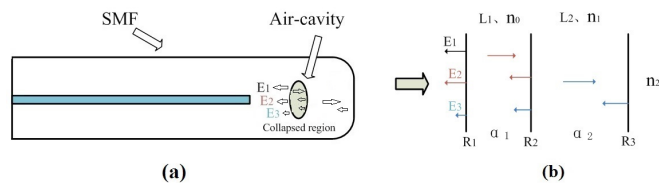


Fig. 2. (a) Structure of the sensor head, and (b) schematic diagram of the reflection model.

is used to illuminate the fiber-tip sensor, and an optical spectrum analyzer (OSA, YOKOGAWA, AQ6370B) is used to monitor the reflection spectrum *in situ* with a wavelength resolution and scanning range of 0.04 and 1255–1335 nm, respectively. The sensor head is dipped into the liquid whose RI is to be measured. For comparison, the reflection spectra of the sensor head in air and water are recorded by OSA, as shown in Fig. 3(b). The fringe contrast decreases when the sensor head is immersed in water, which is found to agree with the theoretically calculated results based on Eq. (2).

To evaluate the capability of RI measurement, the FP fiber-tip sensor was tested using different mass concentrations of glycerol in water. We have prepared seven different concentrations of 0%, 10%, 20%, 30%, 40%, 50% and 60%, whose corresponding RIs are 1.333,

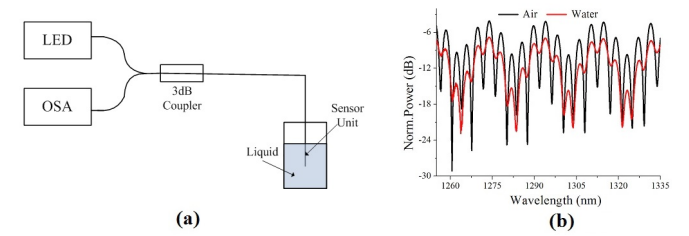


Fig. 3. (a) Schematic diagram of the experimental setup and (b) reflection spectra of the sensor head in air and water.

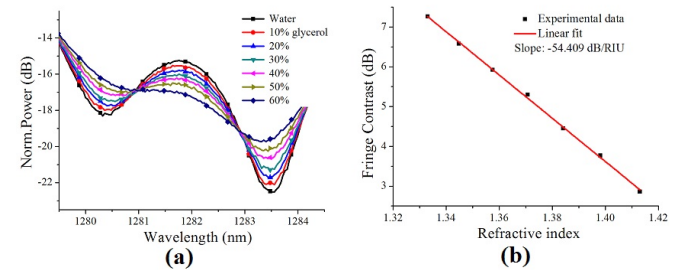


Fig. 4. (a) Measured spectral response to different concentrations of glycerol solution and (b) fringe contrast varies with different RIs.

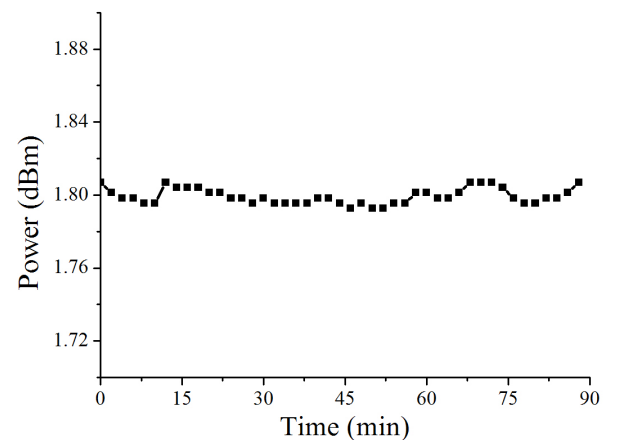


Fig. 5. Power stability of the light source.

1.3448, 1.3575, 1.3707, 1.3841, 1.3981 and 1.413, respectively, at room temperature. The measured reflection spectra are recorded. Fig. 4(a) shows the fringe contrasts of the peak and valley wavelengths at 1282 and 1283.5 nm. It is observed that the fringe contrast decreases as the glycerol solution concentration increases. Fig. 4(b) shows the fringe contrast corresponding to different RIs, where a linear fit of the experimental data is implemented with a high sensitivity of  $-54.409$  dB/refractive index unit (RIU). Over the RI range from 1.333 to 1.413, the fringe contrast varies almost linearly. The RI resolution is limited by two main factors: the amplitude resolution of OSA (0.001 dB in our experiment) and the stability of the light source<sup>[10]</sup>.

Figure 5 shows the stability of the light source in an hour and a half. We can also observe that the power stability of the light source is  $\pm 0.01$  dB, greater than the amplitude resolution of OSA. As a result, the accuracy of the sensor is limited by the stability of the light source.

In conclusion, we propose and fabricate a simple F-P fiber-tip sensor based on an inner air cavity for RI sensing. The sensor head is fabricated by simple splicing and cleaving. The fringe contrast of the interference spectra is modulated by the external RI. Experimental results demonstrate that such an F-P fiber sensor is used as an RI sensor with a sensitivity of  $-54.409$  dB/RIU. It shows the advantages of simple fabrication, low cost, stable and reliable.

This work was finally supported by the Project of National Science Foundation of China, NSFC (No. 51175393), the Fundamental Research Funds for the Central Universities and Self-determined and Innovative Research Funds of WUT (No. 2013-ZY-014).

## References

1. J. Tian, Y. Lu, Q. Zhang, and M. Han, *Opt. Express* **21**, 6633 (2013).
2. Y. J. Rao, M. Deng, D. W. Duan, and T. Zhu, *Sensors Actuators A* **148**, 33 (2008).
3. T. Wei, Y. Han, Y. Li, H. L. Tsai, and H. Xiao, *Opt. Express* **16**, 5764 (2008).
4. T. Wei, Y. Han, H. L. Tsai, and H. Xiao, *Opt. Lett.* **33**, 536 (2008).
5. F. C. Favero, L. Araujo, G. Bouwmans, V. Finazzi, J. Villatoro, and V. Pruneri, *Opt. Express* **20**, 7112 (2012).
6. L. H. Chen, T. Li, C. C. Chan, R. Menon, P. Balamurali, M. Shailender, B. Neu, X. M. Ang, P. Zu, W. C. Wong, and K. C. Leong, *Sensors Actuators B* **169**, 167 (2012).
7. T. Wang and M. Wang, *IEEE Photon. Technol. Lett.* **24**, 1733 (2012).
8. D. J. J. Hu, Y. Wang, J. L. Lim, T. Zhang, K. B. Milen'ko, Z. Chen, M. Jiang, G. Wang, F. Luan, P. P. Shum, Q. Sun, H. Wei, W. Tong, and T. R. Wolin'ski, *IEEE Photon. Technol. Lett.* **12**, 1239 (2012).
9. B. Dong, J. Hao, T. Zhang, and J. L. Lim, *Sensors Actuators B* **171**, 405 (2012).
10. Z. L. Ran, Y. J. Rao, W. J. Liu, X. Liao, and K. S. Chiang, *Opt. Express* **16**, 2252 (2008).